

# Comparing the Performance of OFDM and OCDM-based Visible Light Communications: Numerical and Experimental Analysis

Augusto C. F. Peterle , Wesley Costa , Higor Camporez , Marcelo Segatto , Helder Rocha ,  
Jair A. L. Silva 

LabTel, Electrical Engineering Department, Federal University of Espírito Santo, Vitória-ES, Brazil  
[augusto.peterle@edu.ufes.br](mailto:augusto.peterle@edu.ufes.br), [wesley.costa.55@edu.ufes.br](mailto:wesley.costa.55@edu.ufes.br), [higor.camporez@edu.ufes.br](mailto:higor.camporez@edu.ufes.br),  
[marcelo.segatto@ufes.br](mailto:marcelo.segatto@ufes.br), [helder.rocha@ufes.br](mailto:helder.rocha@ufes.br), [jair.silva@ufes.br](mailto:jair.silva@ufes.br)

**Abstract**— Numerical and experimental analysis of visible light communication (VLC) systems based on orthogonal chirp division multiplexing (OCDM) and orthogonal frequency division multiplexing (OFDM) are presented in this paper. Unlike most of the related publications, in this work we numerically compared OCDM and OFDM based VLC systems with the same equalization process, i.e., employing an one tap equalizer (OTE) in both systems. Simulation results in line-of-sight VLC channels show that both systems have the same performance when baseband multicarrier signals are used. The impact of the optical modulation index and the bias current of a previously characterized light-emitting diode were also evaluated. Nevertheless, the experimental demonstrations, in which bandpass signals were used due to the bandpass characteristic of the exploited setup, show that OFDM-based system outperforms the VLC links with OCDM signals, when the OTE equalizer is used in both systems. The performance of the OCDM-based system was improved by using a zero forcing frequency domain equalizer.

**Index Terms**— Visible light communication, OCDM, OFDM, Equalization.

## I. INTRODUCTION

The recent significant increase in electronic devices connectivity paved the way to the so called “radio frequency spectrum crunch”. Some authors proposed visible light communication (VLC) systems to reach the demand for connections [1]. VLC describes optical wireless systems in which wavelengths around 400-700 nm and light emitting diodes (LEDs) normally used for illumination are implemented [2]. It offer low energy consumption and communication security in short link distances using the unlicensed spectrum. Because it does not affect the functionality of highly sensitive electronics, it has been proposed in critical applications like hospital intensive care units, airplanes, Industry 4.0, among others [3]. Due to the significantly lower energy consumption, LEDs have gained new production methods that resulted in the reduction in their cost [4]. A lower cost and their popularization strongly encourages the implementation of VLC systems, in which high spectral efficiency (SE) can be obtained with OFDM [5].

However, OFDM-based VLC systems requires real valued signals, normally obtained with the adoption of the Hermetian symmetry that halves the SE [6]. An alternative approach to OFDM is the orthogonal chirp division multiplexing (OCDM). The chirps using in OCDM are designed to provide robustness against effects such as noise, multipath fading and Doppler [7]. The OCDM consists of

several orthogonal chirps also used to attain the SE requirement. Nevertheless, experimental performance evaluations that considers the adoption of this multicarrier format in VLC systems remains an issue, especially when the complexity of the equalization process is somehow take into account [8]. In [7], and like in almost all related publications, the authors compared OCDM-based systems using minimum mean square error (MMSE) equalization with OFDM-based systems using one tap equalization. In their works, the OCDM-based system outperforms the OFDM-based system because, unlike with MMSE equalizers, the one tap equalizer (OTE) significantly enhances noise. Therefore, we conjectured that, for the sake of fairness, the performance comparison should be conducted when both above-mentioned VLC systems employs OTE in the equalization process. The OTE choice is due to the complexity reduction, when compared to the MMSE procedure.

This paper is an extension of [9], where, through numerical simulations, we compared the performance of OFDM and OCDM-based VLC systems, considering OTE in both. The simulation results show that the systems had the same performance in line-of-sight (LOS) scenarios, and with an LED model well accepted in the literature [10]. The same performance behaviour occurred in the evaluations of the impact of the optical modulation index and the bias current of a previously experimentally characterized LED. However, it should be stressed that, in the numerical evaluations described in [9], we considered VLC systems with baseband multicarrier signals. Therefore, the novel technical contribution in this paper lies in an experimental validation of the above-mentioned comparison. In particular, it is demonstrated that, with bandpass signals demanded by the frequency response of the exploited setup, the OCDM-based system using OTE produced large values of error vector magnitude (EVM), which led to the adoption of the zero forcing frequency domain equalizer (FDE) proposed in [7], aiming at performance enhancements. The experimental results show that the performance of both systems are almost the same, when the OTE and the FDE equalizers are used in the OFDM and OCDM based systems, respectively.

## II. VLC CHANNEL MODEL

The LOS channel model considered in this work is illustrated in Fig. 1.a). It consists of a transmitter in which the light emission is provided by an LED and a receiver that detects the light by a photodetector. The model considers the LED curve shown in Fig. 1.a) and the system noise is modelled as an additive white Gaussian noise (AWGN) inserted in the receiver [11].

The luminous flux produced by a current flowing through the LED can be defined as

$$P_t = \frac{I_{LED}}{\left( \zeta + \left( \frac{I_{LED}}{P_{MAX}} \right)^{2k} \right)^{1/2k}} \left( \frac{A}{\eta} \right) \quad (1)$$

where  $I_{LED}$  is the current through the LED,  $P_{MAX}$  is LED maximum power,  $\zeta$  is an adjustment constant,  $k$  is the knee factor,  $A$  is the area that light passes through and  $\eta$  is the efficiency in lm/W. The received optical power is generally determined as  $P_r = H(0)P_t$ , where  $P_t$  is the transmitted optical power and  $H(0)$  is the channel DC gain, given by [12]

$$H(0) = \begin{cases} \frac{(m+1)A}{2\pi d^2} \cos^m(\phi) T_s g(\psi) \cos(\psi), & 0 \leq \psi \leq \psi_c \\ 0, & \psi > \psi_c \end{cases} \quad (2)$$

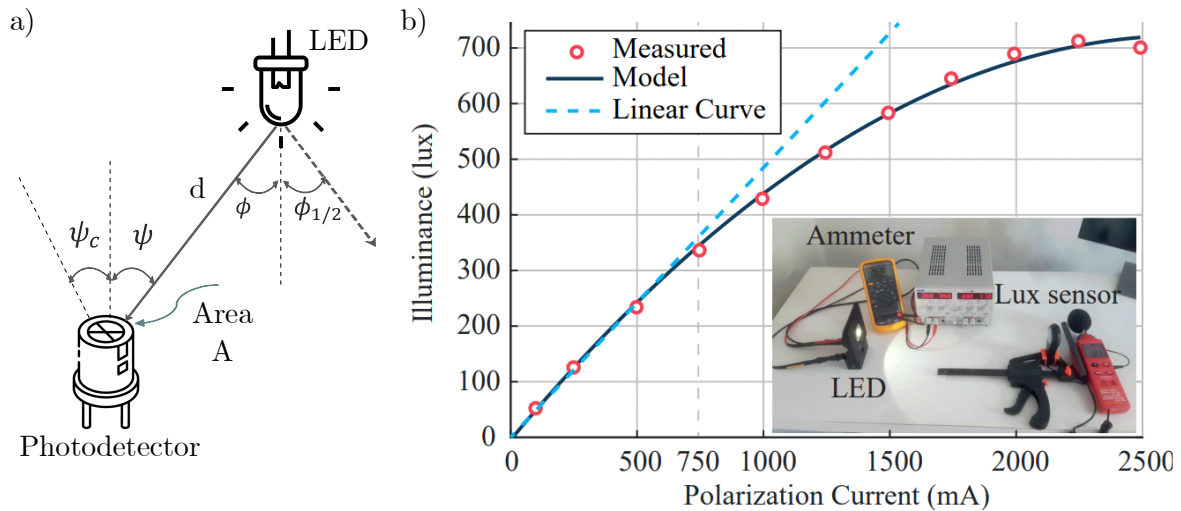


Fig. 1. a) Schematic view of the VLC LOS channel. b) The illuminance versus  $I_{dc}$  curve of the characterized LED.

where  $m$  is the Lambertian factor,  $A$  is the area of the photodetector,  $d$  is the distance between transmitter and receiver,  $T_s$  is the gain of an optical filter,  $g(\psi)$  is the gain of an optical collimator. The electrical current  $I_{LED} = I_{dc} + \alpha \times s(n)$  is composed by the DC component  $I_{dc}$  and a modulating signal  $s(n)$ , for  $\alpha$  a scaling factor obtained as

$$\alpha = \frac{OMI \times I_{MAX}}{OMI + 1}, \quad (3)$$

where  $OMI$  is the modulation index and  $I_{MAX}$  is the maximum current of the LED.

### III. OCDM BASICS

Quadratic phase chirps produce frequencies with linear variations in the time domain. OCDM uses a sequence of quadratic phase chirps orthogonal to each other [7]. These produced chirps occupy the entire bandwidth of the channel and therefore the degradation produced by multipath fading is spread over all the chirps [13]. The sum of several chirps in the time domain provide a peak-to-average power ratio (PAPR) similar to the OFDM system [7], that enforces the strong analogy between such multicarrier formats. In OFDM, the multiplexing and the demultiplexing of the  $N$  subcarriers are performed by inverse and direct fast Fourier transforms, respectively. In OCDM they are performed in the  $N$  subchirps by inverse and direct discrete Fresnel transform (DFnT), respectively. The DFnT is obtained by the DFnT matrix where the inputs are the Talbot coefficients determined as

$$\Phi(p, q) = \frac{1}{\sqrt{N}} e^{-j\frac{\pi}{4}} \begin{cases} e^{j\frac{\pi}{N}(p-q)^2}, & N \equiv 0 \pmod{2} \\ e^{j\frac{\pi}{N}(p+\frac{1}{2}-q)^2}, & N \equiv 1 \pmod{2}, \end{cases} \quad (4)$$

where the operation  $mod$  returns the remainder of an integer division. The  $mod 2 \equiv 0$  represents an even number of  $N$  subchirps, whereas  $mod 2 \equiv 1$  represents an odd number.

### A. OCDM Transmission

The DF<sub>n</sub>T matrix presented in Equation (4) denotes a  $N$  size square matrix and each  $p$  and  $q$  values are row and column. With the DF<sub>n</sub>T matrix, the OCDM symbol can be obtained as following

$$s(n) = \Phi^H x(n), \quad (5)$$

in which  $\Phi^H$  is the Hermitian transpose, i.e., it is the IDF<sub>n</sub>T analogous to the IFFT in OFDM,  $x$  is a vector composed by M-QAM, M-PSK or M-PAM symbols. It can be observed from Equations (4) and (5) that the modulated signal  $s(n)$  have complex values. Nevertheless, in the OCDM approach the Hermitian symmetry cannot be used to output only real signals. According to [14], for baseband signals is possible to handle only real signals by an in-phase and quadrature (I/Q) separation performed in two steps: (i) the  $\Phi_N^H$  performs a IDF<sub>n</sub>T and, (ii) the  $I/Q_{2N}$  performs the I/Q separation, taking thereafter the real part of the first  $N$  values, and the imaginary part of the last  $N$  values.

Due to the frequency response of the our VLC setup [see Fig. 2.b)], in which very low frequencies are attenuated, another strategy was adopted to handle only real signals. As suggested in [15], a digital upconverter (DUC) was employed to convert a baseband signals to passband signals, as shown in Fig. 2.a.I). Thus, the baseband  $s(n)$  signals are upsampled before a lowpass filtering used to remove the spectrum copies, followed by the analog modulation depicted in Fig. 2.a.I).

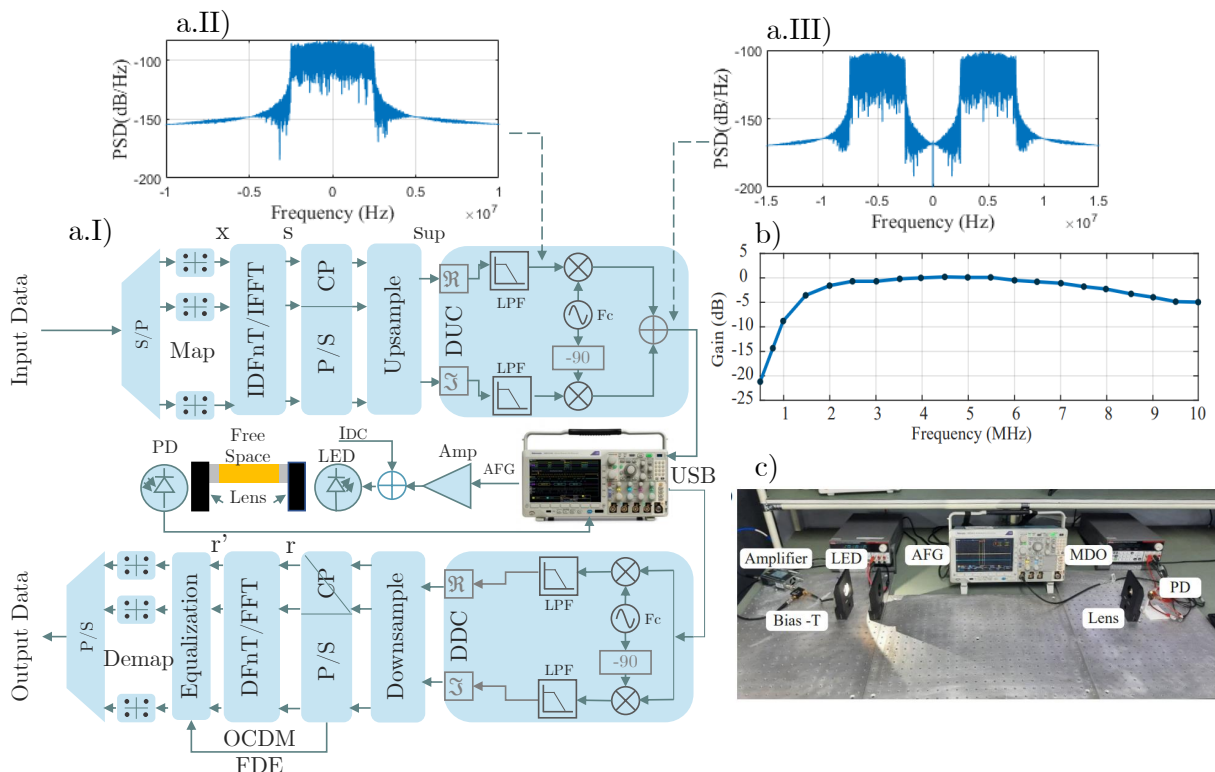


Fig. 2. (a.I) Schematic view of the experimental OCDM/OFDM VLC system setup. (a.II) Upsampled and filtered baseband OCDM signal. (a.III) OCDM passband signal after upconversion. (b) Measured frequency response of the VLC system in back-to-back (B2B). (c) A picture of the components involved in the experiment.

The DUC output is a signal with only real coefficients, centered at the  $F_c$  carrier frequency. This upconverted signal will propagate in the VLC channel through the LED and the photodetector. To avoid clipping of the negative amplitudes of the OCDM signals, a DC current (bias current  $I_{DC}$ ) is added

in the signals before the optical modulation [8], [11]. Fig. 2 also show the shows the demodulation process, as well as a picture of the experimental setup.

### B. OCDM Reception

The digital down converter (DDC) converts the OCDM passband signals to baseband again. The DDC uses the demodulation process shown in Fig 2.a.I), followed by a downsample signal processing. After removing the cyclic prefix, the baseband received OCDM signal  $r(n)$  is obtained. This signal can be mathematically denoted by

$$r(n) = \mathbf{H}s(n) + \eta(n), \quad (6)$$

where  $\eta(n)$  represents the AWGN and  $\mathbf{H}$  the circulant channel impulse response (CIR) matrix where the first column is  $h = [h(0), h(1), \dots, h(N - 1)]^T$ . The  $r'(n)$  signal is the received  $r(n)$  converted back to the time domain by

$$r'(n) = \Phi r(n). \quad (7)$$

In this paper, two equalizers were studied to recover the mapped symbols transmitted. The first one is OTE normally used in common OFDM equalization processes and the second one is zero forcing FDE proposed in [7].

1) **The one tap equalizer (OTE):** To recognize the frequency response used in this equalization, we used 4 training symbols denoted as  $x_p$ . Considering that the receiver knows these symbols [see Fig. 3.a)], and denoting  $r'_p$  as the received training symbols, we obtain a linear vector of  $N \times 1$  channel gains as

$$G_{OTE}(n) = \frac{x_p(n)}{r'_p(n)}. \quad (8)$$

Knowing that, at each one of the 20 transmissions, we transmitted frames composed by 8 multicarrier signals, the equalized symbols of the next 4 signals of each frame were obtained as follows

$$x'(n) = G_{OTE}(n) \times r'(n). \quad (9)$$

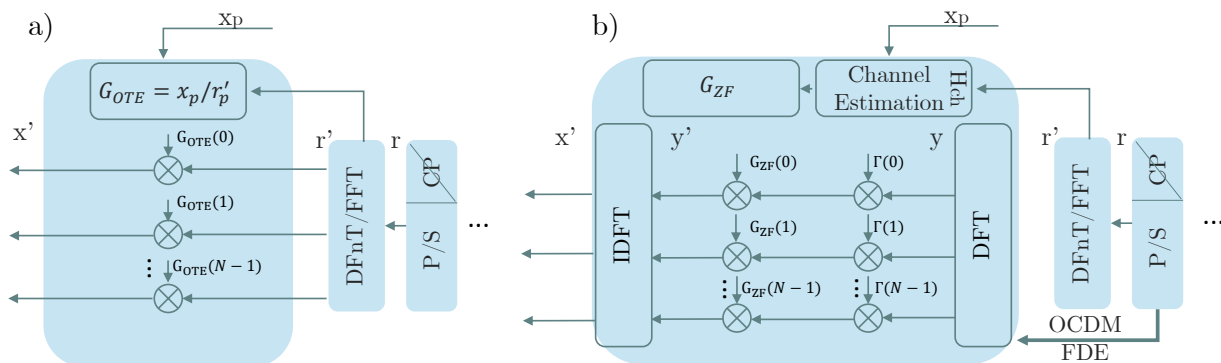


Fig. 3. Block diagram of the two studied equalizers. a) OTE equalizer - training symbols estimates a gain vector  $G_{OTE}$  that compensates the received symbols. b) FDE equalizer - training symbols estimate the channel frequency response,  $\Gamma$  and  $G_{ZF}$  compensates phase and channel effects respectively.

2) **The zero-forcing frequency domain equalizer (FDE):** In the implementation of this equalizer we consider  $\mathbf{F}$  as the normalized  $N \times N$  DFT matrix and  $\mathbf{F}^H$  the DFT matrix Hermitian transpose, i.e., the IDFT matrix. Hence, the channel frequency response (CFR) and the channel impulse response (CIR) can be estimated from

$$H_{ch}(f) = \frac{\mathbf{F} \times r'_p}{\mathbf{F} \times x_p}. \quad (10)$$

Thereafter, the CIR  $h(n)$  can be calculated using the IDFT matrix, generating  $h(n) = \mathbf{F}^H \times H_{ch}$ .

Fig. 3.b) shows that, to execute the equalization, we first perform the DFT of the received signal  $r(n)$  to obtain a vector  $y$  according to

$$y = \mathbf{F} \times r(n) = \mathbf{F} \mathbf{H} \Phi^H x(n) + \mathbf{F} \cdot \eta(n) \quad (11)$$

With the identity matrix  $\mathbf{I} = \mathbf{F}^H \mathbf{F}$  Equation (11) becomes

$$\begin{aligned} y &= \mathbf{F} \mathbf{H} \mathbf{F}^H \mathbf{F} \Phi^H \mathbf{F}^H x + w \\ y &= \mathbf{\Lambda} \mathbf{\Gamma}^H \mathbf{F} x + w, \end{aligned} \quad (12)$$

where  $\mathbf{\Lambda} = \mathbf{F} \mathbf{H} \mathbf{F}^H$  is a diagonal  $N \times N$  CFR matrix with the coefficients of  $H_{ch}$  in the main diagonal. The  $\mathbf{\Gamma}^H = \mathbf{F} \Phi^H \mathbf{F}^H$  is also diagonal but it is the Hermitian transpose of DFNT matrix eigenvalues and  $w$  is the DFT of the channel noise  $\eta$ . The entries of the DFNT matrix eigenvalues  $\mathbf{\Gamma}$  are given by

$$\mathbf{\Gamma}(k) = \begin{cases} e^{-j\frac{\pi}{N}k^2}, & N \equiv 0 \pmod{2} \\ e^{-j\frac{\pi}{N}k(k-1)}, & N \equiv 1 \pmod{2} \end{cases} \quad (13)$$

It can be noted from Equation (12) that, before eliminating the channel contribution, it is first necessary to compensate the phase component  $\mathbf{\Gamma}^H$ , by multiplying  $\mathbf{\Gamma}$ . With the zero forcing criterion  $\mathbf{G}_{ZF}$ , the coefficients are  $\mathbf{G}_{ZF}(k) = \mathbf{\Lambda}^{-1}$ . Therefore the equalized symbols  $x'(n)$  are obtained according to

$$x'(n) = \mathbf{F}^H \mathbf{\Gamma} \mathbf{G} y + \mathbf{F}^H \mathbf{\Gamma} \mathbf{G} w. \quad (14)$$

It can be observed from Equation (14) that the zero forcing equalizer enhances the channel noise.

#### IV. NUMERICAL ANALYSIS

A block diagram of the simulated baseband OCDM-based VLC system model is presented in the Fig. 4. The OCDM symbol has  $N = 512$  subcarriers and the IDFT I/Q outputs 1024 subcarriers. The signals bandwidth used in the simulations is  $B_W = 10$  MHz due to the LED bandwidth limitations. We conducted Monte Carlo simulations to compare the performance of both OFDM and OCDM-based systems through bit-error-rate (BER) against signal-to-noise ratio ( $E_b/N_o$ ), considering different values of  $OMI$ ,  $I_{DC}$  and subcarrier mapping. The white Gaussian noise is added in photodetection.

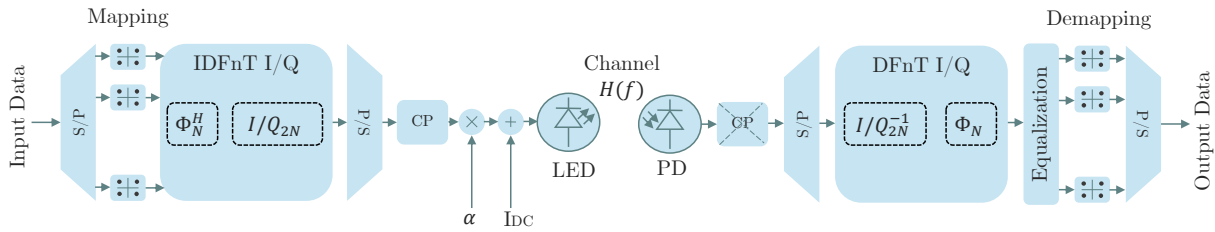


Fig. 4. The OCDM baseband block diagram used in Simulations. To handle only real signals the OCDM baseband has to perform a I/Q separation. In this simulation OCDM and OFDM used the OTE equalizer

Fig. 5a show performance results in terms of BER against  $E_b/N_o$  with a bias current  $I_{DC} = 400$  mA, for both 4 and 16-QAM, and considering values of  $OMI$  equals to 0.1, 0.5 and 0.9. Fig. 5a shows that, in all considered optical modulation indexes, the performance of the OCDM-based VLC system is the same of the system based on OFDM. Fig. 5a also shows that, with 4-QAM mapping, the performance of both VLC systems enhances with the increases in the values of  $OMI$ . This is expected due to the fact that with  $I_{DC} = 400$  mA the LED operates in its linear region (see inset Fig. 1). In this operation region, the impact of the noise decreases with  $OMI$ .

A similar behaviour occurred with 16-QAM, with the exception in the case where  $OMI = 0.9$  is considered. In this case, a performance plateau (BER  $\approx 2 \times 10^{-3}$ ) is registered when for  $E_b/N_o \geq 35$  dB. At low  $I_{DC}$ , the high  $OMI$  and high PAPR produced in both systems provoke clipping that explains the plateau. An alternative solution to this drawback is to increase  $I_{DC}$ , taking into account that large values of  $I_{DC}$  introduce nonlinear effects.

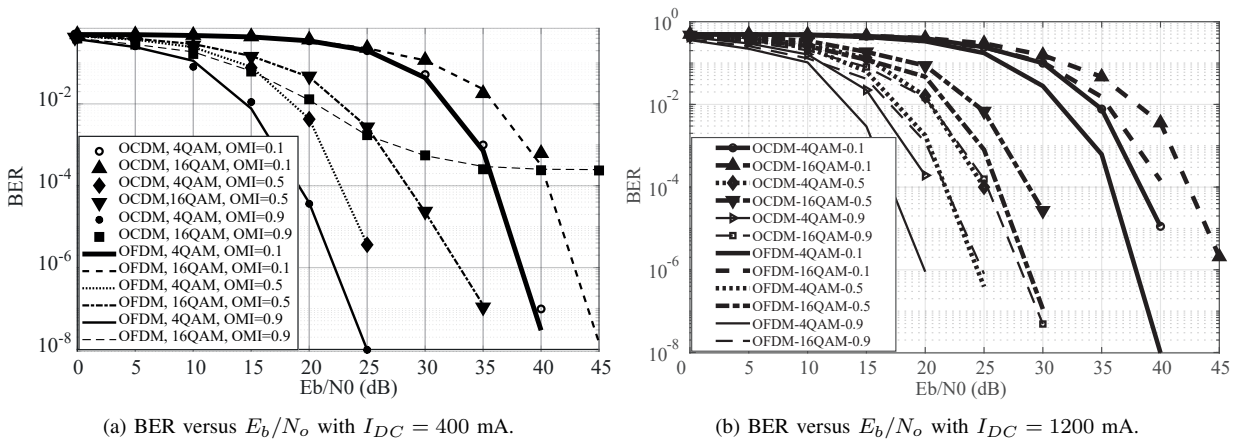


Fig. 5. Performance comparisons between the VLC systems with baseband OCDM and OFDM signals.

Fig. 5b shows the same performance evaluation, however, with a bias current of  $I_{DC} = 1200$  mA. The results depicted in Fig. 5b also show that both VLC systems have almost the same performance. Nevertheless, in this case the plateau is removed due to the increases in  $I_{DC}$ . However, the same performances (when compared with the BER values shown in Fig. 5a) are obtained with higher values of  $E_b/N_o$  due to the clipping phenomena that occurs when the modulating signals (OCDM and OFDM) reaches the nonlinear region of the LED.

In order to emphasize the impact of the LED bias current in the performance of the VLC systems, we also conducted simulations in which the  $I_{DC}$  varied from 100 mA to 2.5 A. Fig. 6 presents the performance comparisons with BER values obtained with  $E_b/N_o = 24$  dB. According, Fig. 6 show that

the performances improve with the optical modulation index. When  $OMI = 0.1$  is considered, the bad performances are almost the same in both systems all over the evaluated range of  $I_{DC}$ , whereas with  $OMI = 0.5$  the performance gradually degrades with values of  $I_{DC}$  greater than 1 A. The scatterplots shown in Fig. 6 illustrate the performances obtained in both systems at  $I_{DC} = 1.2$  A and  $OMI = 0.5$ . It can be verified from Fig. 6 that, for  $OMI = 0.9$ , the performances increase until  $I_{DC} \approx 1.0$  A, from which the performances drastically degrade due to the nonlinearity introduced by the LED.

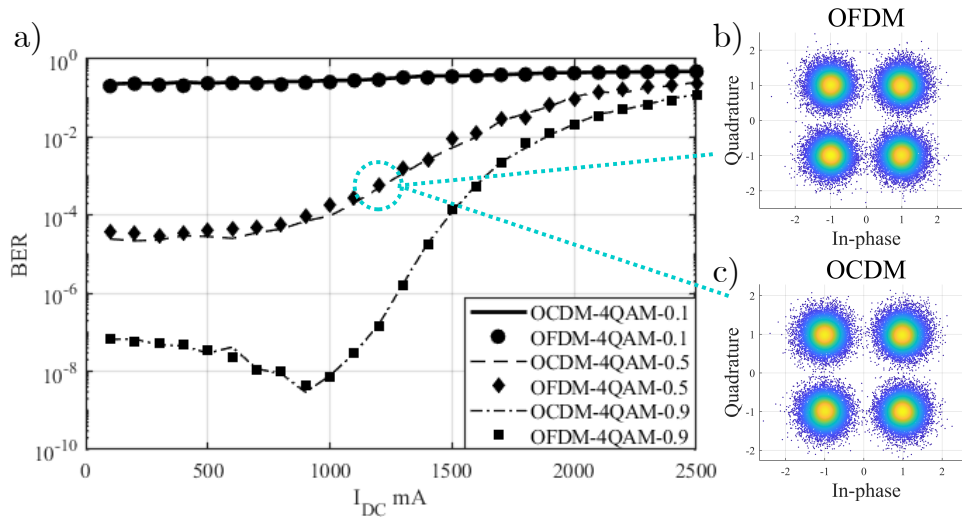


Fig. 6. a) BER versus  $I_{DC}$  with  $E_b/N_o = 24$  dB and 4-QAM. b) OFDM scatter plot at  $I_{DC} = 1200$  mA and  $OMI = 0.5$   
 c) OCDM scatter plot at  $I_{DC} = 1200$  mA and  $OMI = 0.5$

## V. EXPERIMENTAL SETUP

Fig. 2.(a) depicts a block diagram of the experimental setup implemented to evaluate the performance of both OCDM and OFDM based VLC systems. Pseudorandom binary sequences were multiplexed using 64-IDFnT subchirps and 64-IDFnT subcarriers, after mappings with 4 and 16-QAM. At the end of the signal processing using Matlab, a cyclic extension of  $cp = N/8$  was applied to deal with inter-symbol interference, before the upsampling, filtering and modulation procedures above-described. Then the OFDM and OCDM signals were loaded into a 25 MSamples/s arbitrary function generator (AFG). The central frequency chosen for the analog carrier was  $F_c = 5$  MHz to avoid the attenuation observed in the frequency range below 2 MHz shown in Fig. 2.(b). For the same reason, the bandwidth in passband chosen for the analog OCDM signals was  $B_w = 5$  MHz. A summary of the OCDM and OFDM parameterization is presented in Table I.

TABLE I. SUMMARY OF EXPERIMENTAL SETTINGS

Parameter	Variable	OCDM/OFDM
Effective Bandwidth	$B_w$	5 MHz
(I)FFT/(I)DFnT size	$N$	64
Subcarrier mapping	$M$	4-QAM and 16-QAM
Cyclic Prefix	$CP$	$N/8$
Oversampling factor	$K$	5
Central frequency	$F_c$	5 MHz

The analog signals available at the AFG output were amplified and superimposed onto a bias current, aiming to provide non-negative waveforms. The output of the Picosecond Pulse Labs (Model 5575A, bandwidth 12 GHz,  $I_{DC} \leq 500$  mA) Bias-Tee was directly supplied to a commercial LumiLED LXML-PWC2 white LED. After propagation through the LOS channel, supported by bi-convex lenses (optical concentrators), the VLC signals were detected by a HAMAMATSU S10784 photodiode, before analog-to-digital conversion by a 2.5 GSamples/s mixed domain oscilloscope (MDO) and offline signal processing. Fig. 2.(c) depicts a photo of the setup.

## VI. EXPERIMENTAL RESULTS AND DISCUSSIONS

Fig. 7 shows the experimental results in terms of EVM versus link distance for 4-QAM subcarrier/subchirp mapping, and Fig. 8 shows the performance comparisons for 16-QAM. It can be observed in both Fig. 7 and 8 that the OCDM-based VLC systems with OTE have the poorest performance and the OFDM-based system with OTE the best. This is explained by the fact that the OCDM signals are quadratic phase signals and the OTE equalizer does not compensate the phase dispersion effects that occur when the signals are oversampled, filtered and upconverted. Therefore, to approximate the performance of the OCDM-based systems with the ones with OFDM and OTE, we adopted the zero-forcing FDE above-described in the VLC systems with OCDM signals.

Fig. 7.a) shows that, even with a bad equalization with the OTE, the EVM values of the OCDM-based systems were below the forward error correction (FEC) limit. In the 4-QAM case the FEC limit is  $EVM = 17.5\%$ , which is considered as a coding threshold at a  $BER = 3.8 \times 10^{-3}$  and the FEC decoding will correct this raw BER to  $10^{-20}$  [16]. The error free constellation depicted in Fig. 7.b) measured at 100 cm demonstrated the good performance of the system in this scenario. It is also observed from Fig. 7.a) that, when the link distance is close to 175 cm the EVM increases due to losses in the LOS links. As expected, when the link distance decreases the EVM decreases, when the performances measured at 100 cm are used as reference. The constellations shown in Fig. 7.c) and d) demonstrate the extremely good performances of the OCDM and OFDM systems with FDE and OTE, respectively. However, at 25 cm the performance of the OCDM with OTE degrades due to saturation effects in the photodetection. The  $\approx 2\%$  EVM difference between the two systems with the best performances allows the conclusion that the two systems have almost the same performance.

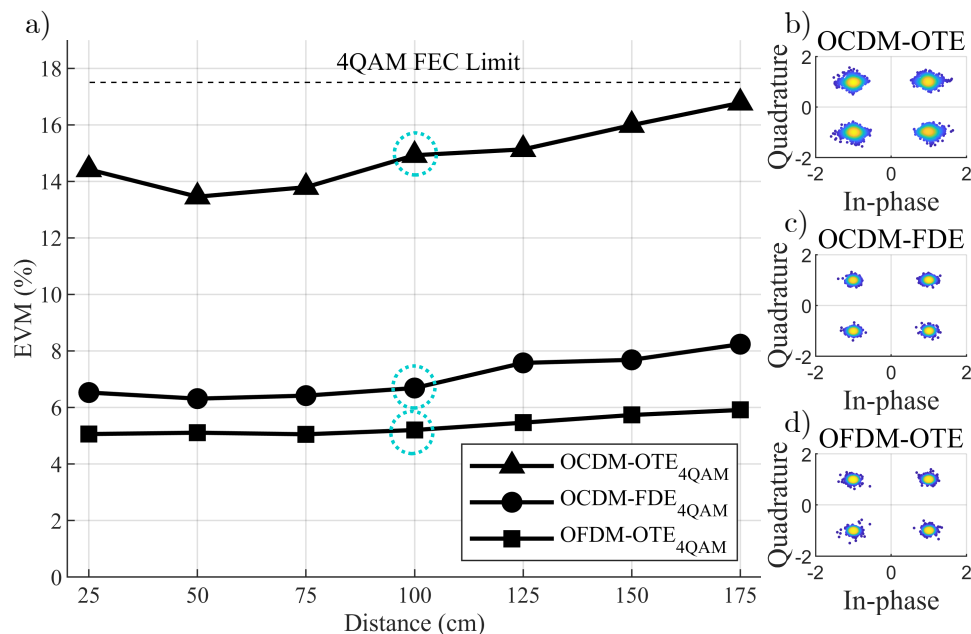


Fig. 7. a) EVM% vs Distance in cm for 4QAM digital mapping. All curves for are below the FEC Limit. Note that OCSDM-OTE showed a big difference in EVM compared to OCSDM-FDE and OFDM. Circled points are shown in constellation diagrams. b),c) and d) shows the OCSDM-OTE, OCSDM-FDE and OFDM-OTE constellations respectively

The results shown in Fig. 8 indicated that, with 16-QAM as subcarrier/subchirp mapping, the OCSDM-OTE provided a bad performance, according to the EVM values above the FEC limit (EVM = 12.5%). The constellation depicted Fig. 8.b) proves this statement. Similar behaviour registered in Fig. 7.a), in terms of performance penalties and photodetector saturation, occurred in this scenario. The constellations depicted Fig. 8.c) and d) demonstrate the extremely good performance of the OFDM and OCSDM-based systems with OTE and FDE, respectively.

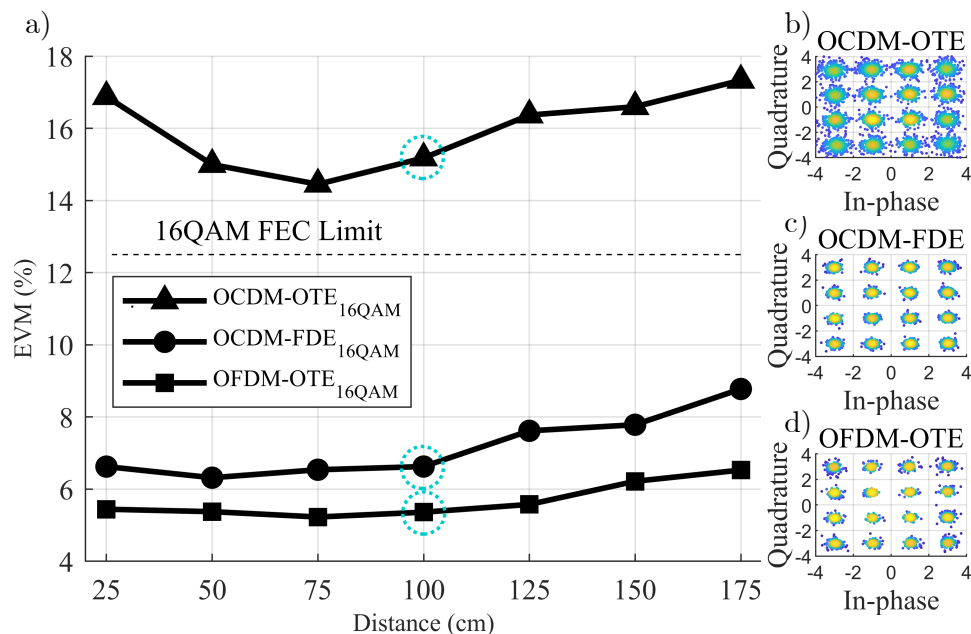


Fig. 8. EVM% vs Distance in cm for 16QAM digital mapping. The OCDM-OTE has an EVM % above the FEC limit, thus presenting transmission errors. OCDM-FDE and OFDM on the other hand have error-free transmission..Circled points are shown in constellation diagrams. b),c) and d) shows the OCDM-OTE, OCDM-FDE and OFDM-OTE constellations respectively

## VII. CONCLUSIONS

The results obtained after the numerical simulations of visible light communication systems based on baseband orthogonal chirp division multiplexing has the same performance of baseband OFDM-based VLC systems in line-of-sight channels. In the numerical analysis, we adopted one tap equalizer in the equalization procedures of both systems. This is in contrast to the related publications in the literature because almost all works compare the performance of OCDM using minimum mean square error equalization with OFDM employing one tap equalizers. Moreover, our results show that relatively large values of OMI can be adopted to address the impact of noise, although an extra concern in the LED bias current should be considered due to nonlinearities and clipping.

On the other hand, the practical experiment showed that OFDM-based VLC systems with one tap equalizer outperforms the OCDM-based systems with the same equalizer. The experimental results also show that the performance of the VLC links approximate to the performance of the above-mentioned OFDM systems, when a zero forcing frequency domain equalizer is employed. Optimization algorithms can be implemented in both systems to further improve their performances. Analysis in multiple-input and single-output channels is part of our future works.

## REFERENCES

- [1] L. E. M. Matheus, A. B. Vieira, L. F. Vieira, M. A. Vieira, and O. Gnawali, "Visible light communication: concepts, applications and challenges," *IEEE Communications Surveys & Tutorials*, vol. 21, no. 4, pp. 3204–3237, 2019.
- [2] S. Rajagopal, R. D. Roberts, and S.-K. Lim, "Ieee 802.15. 7 visible light communication: modulation schemes and dimming support," *IEEE Communications Magazine*, vol. 50, no. 3, 2012.
- [3] A.-M. Căilean and M. Dimian, "Current challenges for visible light communications usage in vehicle applications: A survey," *IEEE Communications Surveys & Tutorials*, vol. 19, no. 4, pp. 2681–2703, 2017.

- [4] H. F. Chinchero, J. M. Alonso, and H. Ortiz, "Led lighting systems for smart buildings: a review," *IET Smart Cities*, vol. 2, no. 3, pp. 126–134, 2020.
- [5] P. H. Pathak, X. Feng, P. Hu, and P. Mohapatra, "Visible light communication, networking, and sensing: A survey, potential and challenges," *IEEE communications surveys & tutorials*, vol. 17, no. 4, pp. 2047–2077, 2015.
- [6] A. A. Abdulkafi, M. Y. Alias, and Y. S. Hussein, "Performance analysis of dco-ofdm in vlc system," in *2015 IEEE 12th Malaysia International Conference on Communications (MICC)*, pp. 163–168, 2015.
- [7] X. Ouyang and J. Zhao, "Orthogonal chirp division multiplexing," *IEEE Transactions on Communications*, vol. 64, no. 9, pp. 3946–3957, 2016.
- [8] F. T. Monteiro, W. S. Costa, J. L. Neves, D. M. Silva, H. R. Rocha, E. O. Salles, and J. A. Silva, "Experimental evaluation of pulse shaping based 5g multicarrier modulation formats in visible light communication systems," *Optics Communications*, vol. 457, p. 124693, 2020. [Online]. Available: <https://www.sciencedirect.com/science/article/pii/S0030401819308946>
- [9] A. C. F. Peterle, W. Costa, H. Camporez, M. Segatto, H. Rocha, and J. A. L. Silva, "Orthogonal chirp division multiplexing in visible light communication: A performance comparison with ofdm-based systems," in *2021 SBMO/IEEE MTT-S International Microwave and Optoelectronics Conference (IMOC)*, pp. 1–3, 2021.
- [10] H. Elgala, R. Mesleh, and H. Haas, "An led model for intensity-modulated optical communication systems," *IEEE Photonics Technology Letters*, vol. 22, no. 11, pp. 835–837, 2010.
- [11] K. M. vd Zwaag, J. L. Neves, H. R. Rocha, M. E. Segatto, and J. A. Silva, "Adaptation to the leds flicker requirement in visible light communication systems through ce-ofdm signals," *Optics Communications*, vol. 441, pp. 14–20, 2019. [Online]. Available: <https://www.sciencedirect.com/science/article/pii/S003040181930121X>
- [12] K. Cui, G. Chen, Z. Xu, and R. D. Roberts, "Line-of-sight visible light communication system design and demonstration," in *2010 7th International Symposium on Communication Systems, Networks Digital Signal Processing (CSNDSP 2010)*, pp. 621–625, 2010.
- [13] Z. Hu, X. Ouyang, J. Zhao, P. Townsend, and C.-K. Chan, "Investigation of a low-complexity transceiver for orthogonal chirp division multiplexing based im/dd owc systems," in *2019 24th OptoElectronics and Communications Conference (OECC) and 2019 International Conference on Photonics in Switching and Computing (PSC)*, pp. 1–3, 2019.
- [14] L. de M. B. A. Dib, G. R. Colen, M. de L. Filomeno, and M. V. Ribeiro, "Orthogonal chirp division multiplexing for baseband data communication systems," *IEEE Systems Journal*, vol. 14, no. 2, pp. 2164–2174, 2020.
- [15] X. Ouyang, G. Talli, M. J. Power, and P. D. Townsend, "Orthogonal chirp-division multiplexing for im/dd-based short-reach systems," *Optics express*, vol. 27 16, pp. 23 620–23 632, 2019.
- [16] R. Schmogrow, B. Nebendahl, M. Winter, A. Josten, D. Hillerkuss, S. Koenig, J. Meyer, M. Dreschmann, M. Huebner, C. Koos, J. Becker, W. Freude, and J. Leuthold, "Error vector magnitude as a performance measure for advanced modulation formats," *IEEE Photonics Technology Letters*, vol. 24, no. 1, pp. 61–63, 2012.